Peering towards Cosmic Dawn
Proceedings IAU Symposium No. 333, 2018
V. Jelić & T. van der Hulst, eds.

doi:10.1017/S1743921317011280

The angular power spectrum measurement of the Galactic synchrotron emission using the TGSS survey

Samir Choudhuri[1,2], Somnath Bharadwaj[2], Sk. Saiyad Ali[3], Nirupam Roy[4], H. T. Intema[5] and Abhik Ghosh[6,7]

[1]National Centre For Radio Astrophysics, Post Bag 3, Ganeshkhind, Pune 411 007, India
[2]Department of Physics, & Centre for Theoretical Studies, IIT Kharagpur, Kharagpur 721 302, India
[3]Department of Physics,Jadavpur University, Kolkata 700032, India
[4]Department of Physics, Indian Institute of Science, Bangalore 560012, India
[5]Leiden Observatory, Leiden University, Niels Bohrweg 2, NL-2333CA, Leiden, The Netherlands
[6]Department of Physics and Astronomy, University of the Western Cape, Robert Sobukwe Road, Bellville 7535, South Africa
[7]SKA SA, The Park, Park Road, Pinelands 7405, South Africa

Abstract. Characterizing the diffuse Galactic synchrotron emission (DGSE) at arcminute angular scales is needed to remove this foregrounds in cosmological 21-cm measurements. Here, we present the angular power spectrum (C_ℓ) measurement of the diffuse Galactic synchrotron emission using two fields observed by the TIFR GMRT Sky Survey (TGSS). We apply 2D Tapered Gridded Estimator (TGE) to estimate the C_ℓ from the visibilities. We find that the residual data after subtracting the point sources is likely dominated by the diffuse Galactic synchrotron radiation across the angular multipole range $240 \leqslant \ell \lesssim 500$. We fit a power law to the measured C_ℓ over this ℓ range. We find that the slopes in both fields are consistent with earlier measurements. For the second field, however, we interpret the measured C_ℓ as an upper limit for the DGSE as there is an indication of a significant residual point source contribution.

Keywords. methods: statistical, data analysis - techniques: interferometric- cosmology: diffuse radiation

1. Introduction

Observations of the redshifted neutral hydrogen (HI) 21-cm radiation can be used to probe a wide range of cosmological and astrophysical phenomena over a large redshift range $0 < z \lesssim 200$ (Bharadwaj & Ali 2005; Pritchard & Loeb 2012; Mellema *et al.* 2013). There are several ongoing and future experiments such as the Donald C. Backer Precision Array to Probe the Epoch of Reionization (PAPER,Parsons *et al.* 2010), the Low Frequency Array (LOFAR, van Haarlem *et al.* 2013; Yatawatta, *et al.* 2013) and the Murchison Wide-field Array (MWA, Bowman *et al.* 2013; Tingay *et al.* 2013), the Square Kilometer Array (SKA1 LOW, Koopmans *et al.* 2015) and the Hydrogen Epoch of Reionization Array (HERA, Neben, *et al.* 2016) which are aiming to detect the power spectrum of the 21-cm signal from the Epoch of Reionization (EoR, $6 \lesssim z \lesssim 13$). The main challenges for detecting the cosmological 21-cm signal are the astrophysical foregrounds which are $4 - 5$ orders of magnitude brighter than the expected signal (Shaver *et al.* 1999; Santos, Cooray & Knox 2005; Ali, Bharadwaj & Chengalur 2008). The major foreground components include the point sources, diffuse Galactic synchrotron emission, Galactic and extra-galactic free-free emission. The diffuse Galactic synchrotron emission

(DGSE) is the most dominant foreground component at large angular scale. The detailed understanding of the DGSE is needed to remove this component in 21-cm experiments. The study of the DGSE also quantifies the fluctuations in the magnetic field and in the electron density of the turbulent interstellar medium (ISM) of our Galaxy (e.g. Waelkens, Schekochihin & Enßlin 2009; Lazarian & Pogosyan 2012; Iacobelli *et al.* 2013).

Several observations are made to characterize the DGSE at wide frequency range. Haslam *et al.* (1982) have quantified the all-sky diffuse Galactic synchrotron radiation at 408 MHz. Reich (1982) and Reich & Reich (1988) have observed the Galactic synchrotron emission at higher frequency (1.4 GHz). Guzmán *et al.* (2011) have studied all-sky temperature variation at 45 MHz using Maipu and Muradar array and also measured the spectral index by comparing this with Haslam *et al.* (1982) 408 MHz map. Dowell *et al.* (2017) have presented the low-frequency all-sky map between 35 MHz to 80 MHz. Bernardi *et al.* (2009) have estimated the C_ℓ using Westerbork Synthesis Radio Telescope (WSRT) observations and found that it follows a power law power spectrum up to multipole range $\ell \leqslant 900$. Ghosh *et al.* (2012) have analyzed GMRT 150 MHz data and estimated the C_ℓ from the residual data. For both cases the slope of the measured C_ℓ is in the range $\beta = 2$ to 3. Recently, Iacobelli *et al.* (2013) reported that the C_ℓ of the foreground synchrotron fluctuations is approximately a power law with a slope $\beta \approx 1.8$ up to angular multipoles of 1300.

Here, we present the C_ℓ measurement of the DGSE using two fields observed by the TIFR GMRT Sky Survey (TGSS†; Sirothia *et al.* 2014). We use the data from TGSS-ADR survey Intema *et al.* (2017) and apply the Tapered Gridded Estimator (TGE; Choudhuri *et al.* 2016) to the residual data to measure the C_ℓ. We identify the angular multipole range where the measured C_ℓ is likely dominated by the DGSE, and we present power law fits in this region.

2. Data Analysis

We use two data sets from the TGSS survey and estimated the C_ℓ for them. The Galactic coordinates for these fields are $(9^\circ, +10^\circ$; **Data1**) and $(15^\circ, -11^\circ$; **Data2**). The central frequency of this survey is 147.5 MHz with an instantaneous bandwidth of 16.7 MHz. These data sets were analysed with a fully automated pipeline based on the SPAM package (Intema *et al.* 2009; Intema 2014). The off source rms noise (σ_n) for these fields are 4.1 mJy/Beam and 3.1 mJy/Beam for **Data1** and **Data2** respectively. We subtract all bright point sources from the central region of the telescope's primary beam to characterize the underlying diffuse emission.

We apply the TGE to estimate C_ℓ from the measured visibilities $\mathcal{V}_i$. The TGE incorporates three novel features. First, the estimator uses the gridded visibilities to make it computationally much faster. Second, a positive noise bias is removed by subtracting the auto-correlation of the visibilities. Third, the estimator allows us to taper the primary beam so as to restrict the contribution from the sources in the outer regions and the sidelobes. The details are discussed in Choudhuri *et al.* 2014, 2016. The tapering is introduced by multiplying the sky with a window function. $\mathcal{W}(\theta) = e^{-\theta^2/\theta_w^2}$. Here, we implement the tapering by convolving the measured visibilities with Fourier transform of the window function. We have used the TGE to estimate C_ℓ and its variance in bins of equal logarithmic interval in ℓ. In this work we correct each baseline with proper frequency scaling and finally collapse all channels to estimate the C_ℓ.

† http://tgss.ncra.tifr.res.in

https://doi.org/10.1017/S1743921317011280 Published online by Cambridge University Press

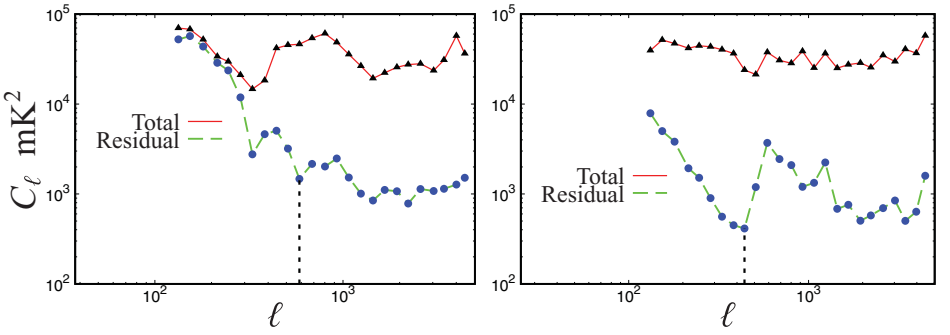

Figure 1. The estimated C_ℓ for **Data1** and **Data2** are shown in the left and right panel respectively. The upper and lowers curves are for before and after suntracting the point sources respectively. We identify a region shown by the vertical dotted lines in both panels ($\ell \geqslant \ell_{max}$) after which the residual C_ℓ is dominated by unsubtracted point sources. This figure is taken from Choudhuri *et al.* 2017.

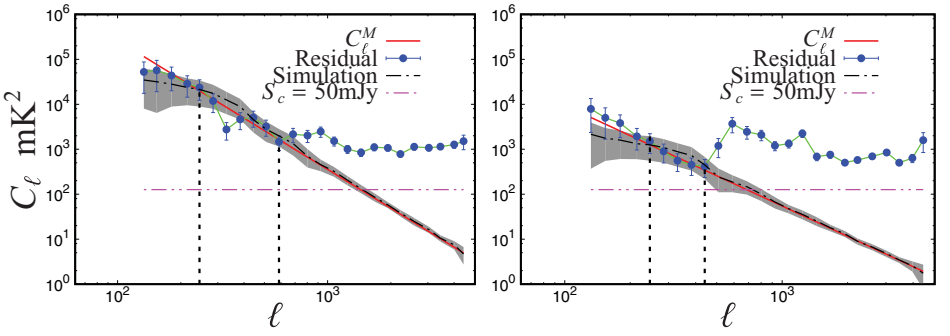

Figure 2. The estimated C_ℓ from the residual data (solid circles) with 1σ error bar for **Data1** is shown in the left panel. Two vertical lines are to show the region where the DGSE is expected to be dominated. The C_ℓ using the best fit parameters is shown by the solid line. The simulated C_ℓ using the best fit parametes is shown by the dash-dot line and the corresponding $1-\sigma$ error is shown with shaded region. The theoretical prediction for the C_ℓ due to residual point sources upto flux density $S_c = 50$mJy is shown by dot-dot-dash line. The right panel shows the same but for **Data2**. This figure is taken from Choudhuri *et al.* 2017.

3. Results and Conclusions

Figure 1 shows the estimated C_ℓ before and after subtracting the point sources from the central region of the primary beam. The left and right panels of Figure 1 are for **Data1** and **Data2** respectively. The upper curves in this figure show the C_ℓ before subtracting any point sources from the data. For both data sets the measured C_ℓ is in the range $10^4 - 10^5$ mK^2 for all values of ℓ. The estimated C_ℓ is mainly dominated by the combination of the point sources and diffuse Galactic synchrotron emission. The lower curves in this figure show the measured C_ℓ after subtracting the point sources from the data. we subtract all the point sources upto $5\sigma_n$ cut off level from the central region of the FoV. The estimated C_ℓ in lower ℓ values are affected by the convolution primary beam (Figure 3, Choudhuri *et al.* 2014). At large ℓ, the residual C_ℓ is mainly dominated by the unsubtracted point sources. We identify a region in the ℓ space $\ell \leqslant \ell_{max}$ ($\ell_{max} = 580$ and 440 for **Data1** and **Data2** respectively) where we believe the diffuse Galactic synchrotron emission has a significant contribution. The left and right panels of Figure 2 show the residual C_ℓ with $1-\sigma$ error bar for **Data1** and **Data2** respectively. Two vertical lines in these figures show the region (ℓ_{min}, ℓ_{max}) where we expect the estimated C_ℓ is likely

https://doi.org/10.1017/S1743921317011280 Published online by Cambridge University Press

dominated by the Galactic synchrotron emission. The estimated C_ℓ behaves as a power law in this region. We fit a power law, $C_\ell = A \times \left(\frac{1000}{l}\right)^\beta \mathrm{mK}^2$ to the measured C_ℓ in this ℓ range. The best fits values of (A, β) are $(356.23 \pm 109.5, 2.8 \pm 0.3)$ and $(54.6 \pm 26, 2.2 \pm 0.4)$ for **Data1** and **Data2** respectively. The values of β from this analysis are quite consistent with earlier measurements (Bernardi *et al.* 2009; Ghosh *et al.* 2012; Iacobelli *et al.* 2013). In Figure 2, we have also shown the C_ℓ using the simulated data. In this simulation, we have used best-fit values of A and β. The $1-\sigma$ errors for the simulated C_ℓ, estimated using 128 independent realizations, are also shown by a shaded region. We have shown the theoretical prediction for the C_ℓ due to residual point sources in a situation where the all bright sources of flux density $S > 50$ mJy has been subtracted from the data. In our analysis, the measured C_ℓ at $\ell > \ell_{max}$ is somewhat overestimated as compared with the theoretical prediction. It may be due to the error in modelling and subtracting point sources from the central region.

In summary, we have estimated the angular power spectrum C_ℓ using two fields observed by TGSS in the ℓ range $150 \leqslant \ell \leqslant 4000$. We identify the region in ℓ space $(240 \leqslant \ell \lesssim 500)$ which we expect to be dominated by the DGSE. We present a power law fits to the estimated C_ℓ over this ℓ range. The best fit values of the amplitude (A) and the power law index (β) are $(356.23 \pm 109.5, 2.8 \pm 0.3)$ and $(54.6 \pm 26, 2.2 \pm 0.4)$ for two data sets considered here. The values of β are consistent with the earlier measurements. We plan to extend this analysis for the whole sky and study the variation of the amplitude (A) and power law index (β) of C_ℓ using the full TGGS survey in future.

4. Acknowledgements

S. Choudhuri would like to acknowledge the University Grant Commission, India for providing financial support. S. Choudhuri would also like to thank the organizers of the IAUS 333 conference.

References

Ali, S. S., Bharadwaj, S., & Chengalur, J. N., 2008, *MNRAS*, 385, 2166
Bernardi, G. *et al.* 2009, *AAP*, 500, 965
Bharadwaj, S. & Ali, S. S., 2005, *MNRAS*, 356, 1519
Bowman, J. D. *et al.* 2013, *Pub. Astro. Soc. Australia*, 30, 31
Choudhuri, S., Bharadwaj, S., Ali, S. S., Roy, N., Intema, H. T., & Ghosh A., 2017, *MNRAS*, 470, L11
Choudhuri, S., Bharadwaj, S., Chatterjee, S., Ali, S. S., Roy, N., & Ghosh A., 2016, *MNRAS*, 463, 4093
Choudhuri, S., Bharadwaj, S., Ghosh, A., & Ali, S. S., 2014, *MNRAS*, 445, 4351
Dowell, J., Taylor, G. B., Schinzel, F. K., Kassim, N. E., & Stovall, K., 2017, *MNRAS*, 469, 4537
Ghosh, A., Prasad, J., Bharadwaj, S., Ali, S. S., & Chengalur, J. N., 2012, *MNRAS*, 426, 3295
Guzmán A. E., May, J., Alvarez, H., & Maeda, K., 2011, *AAP*, 525, A138
Haslam, C. G. T., Salter, C. J., Stoffel, H., & Wilson, W. E., 1982, *AAPS*, 47, 1
Iacobelli, M. *et al.* 2013, *AAP*, 558, A72
Intema, H. T., 2014, in *Astronomical Society of India Conference Series*, Vol. 13, Astronomical Society of India Conference Series
Intema, H. T., Jagannathan, P., Mooley, K. P., & Frail, D. A., 2017, *AAP*, 598, A78
Intema, H. T., van der Tol S., Cotton, W. D., Cohen, A. S., van Bemmel I. M., & Röttgering H. J. A., 2009, *AAP*, 501, 1185
Koopmans, L. *et al.* 2015, *Advancing Astrophysics with the Square Kilometre Array (AASKA14)*, 1
Lazarian, A. & Pogosyan, D., 2012, *ApJ*, 747, 5

Mellema, G. *et al.* 2013, *Experimental Astronomy*, 36, 235
Neben, A. R. *et al.* 2016, *ApJ*, 826, 199
Parsons, A. R. *et al.* 2010, *AJ*, 139, 1468
Pritchard, J. R. & Loeb, A., 2012, *Reports on Progress in Physics*, 75, 086901
Reich, P. & Reich, W., 1988, *AAPS*, 74, 7
Reich, W., 1982, *AAPS*, 48, 219
Santos, M. G., Cooray, A., & Knox, L., 2005, *ApJ*, 625, 575
Shaver, P. A., Windhorst, R. A., Madau, P., & de Bruyn A. G., 1999, *AAP*, 345, 380
Sirothia S. K., Lecavelier des Etangs A., Gopal-Krishna, Kantharia N. G., & Ishwar-Chandra C. H., 2014, *AAP*, 562, A108
Tingay, S. J. *et al.* 2013, *Pub. Astro. Soc. Australia*, 30, 7
van Haarlem, M. P. *et al.* 2013, *AAP*, 556, A2
Waelkens, A. H., Schekochihin, A. A., & Enßlin T. A., 2009, *MNRAS*, 398, 1970
Yatawatta, S. *et al.* 2013, *AAP*, 550, A136

https://doi.org/10.1017/S1743921317011280 Published online by Cambridge University Press